IEEE Access
Multidisciplinary | Rapid Review | Open Access Journal

Received February 6, 2020, accepted February 20, 2020, date of publication February 27, 2020, date of current version March 11, 2020.

Digital Object Identifier 10.1109/ACCESS.2020.2976907

An Improved Equivalent Dipole Moment Source Model Based on Regularization Optimization Method for Near Field-Far Field Conversion

WEI LIU, ZHAOWEN YAN, JIANWEI WANG, ZHENG MIN, AND ZHANGQIANG MA
School of Electronic and Information Engineering, Beihang University, Beijing 100191, China

Corresponding author: Zhaowen Yan (yanzhaowen@buaa.edu.cn)

This work was supported in part by the National Natural Science Foundation of China (NSFC) under Grant 61427803 and Grant 61271044, and in part by the Defense Industrial Technology Development Program under Grant JCKY2016601B005.

ABSTRACT The radiation emission from high-speed digital circuit may result in radio-frequency interference (RFI) problems in modern electronic devices. In this paper, an improved equivalent dipole source based on a new transfer model and a new regularization method is proposed. The equivalent source is obtained by solving an inverse equation with near-field data. The tangential component of electric field used in conventional equivalent source extraction is replaced by the normal component, which can reduce the test difficulty and enhance the measurement efficiency. The new regularization method based on Tikhonov and truncated singular value decomposition (TSVD) can enhance the stability and accuracy of the dipole solution. In addition, the new transfer model and regularization method are verified by simulations and measurements.

INDEX TERMS EMC, equivalent dipole source, far-field radiation, near-field scanning, regularization method, source reconstruction.

I. INTRODUCTION

With the development of electronic devices, the compact and complex design may result in drastic radiation emission problems. Source location and EMI estimation have been very important for printed circuit board (PCB) designers and electromagnetic compatibility (EMC) engineers. Due to commercial confidentiality and protective package, it is often impossible to capture the detailed physical size and field distribution of a noise source. Therefore, the simulations in full-wave tools lack sufficient conditions. The research on the source reconstruction has become more attractive [1].

Over the past decades, source reconstruction based on near-field measurements has been paid more attention to both antenna tests and PCB diagnoses [2]–[4]. There are many methods used to extract the equivalent source of a device under test (DUT) based on near-field data. A widely used method is to create an equivalent surface current source based on integral functions and Green's function [5]. As mentioned in [6], a super-resolution source reconstruction method is investigated with free space Green's function. In [7]–[9], the near- and far-field patterns of an antenna can be computed by an equivalent current source. A dipole probes array is used to carry out the near-field to far-field transformation in [10]. In addition, a source reconstruction technique based on near-field data is given in [11] to calculate the forward and backward radiation pattern of an antenna.

Another well-known source reconstruction technique based on electric and magnetic dipoles is mentioned in [12] and [13]. The main research on equivalent dipole source is composed of the plane-wave spectrum theory and the source reconstruction principle [14], [15]. An actual source can be replaced by a set of infinitesimal dipoles of different types, amplitudes, phases, locations and orientations [16]. The dipoles are used to produce a radiation distribution that is equivalent to the radiation distribution created by the target DUT. In addition, the voltage and current on the surface of the DUT can be described by the dipole array respectively. Previous work has shown that this approach can be applied in near-field coupling and far-field radiation of ICs, packages and PCBs [17]. And the research tendency of equivalent dipole source is using less near-field data to enhance the measurement efficient of near-field data [18].

The associate editor coordinating the review of this manuscript and approving it for publication was Mohammad Tariqul Islam.

To accurately locate a noise source, the distance between near-field probe and DUT should be very small, and a high-resolution scanning is necessary for EMI diagnose of a small size PCB. And the perturbation created by near-field probe should be considered. A comparison result is given in appendix to illustrate the perturbation created by different near-field probes. In addition, both the amplitude and phase information of the near-field data are required to obtain an accurate and stable equivalent dipole source [19]. However, the tangential component of electric field is difficult to measure because of the limitation of tangential electric field probe. In contrast, the normal component of an electric field can easily be obtained by a common near-field probe. Therefore, it is time consuming to measure the distribution of a tangential electric field in conventional research.

Meanwhile, the calculation of a dipole array is a common discrete ill-posed inverse problem [20]. To mitigate the effect of ill-posed system, many numerical method and mathematical considerations are mention in [21]. It can be proved that the error of dipole solution is affected by the condition number of transfer matrix [22]. The condition number can be influenced by some factors such as the amounts, the distributions and the locations of the dipoles and measurement points. In conventional research, the selection of transfer matrix is determined by theoretical criterion. And the empirical laws are also helpful for choosing a local optimum transfer matrix.

The least-square is a common method for obtaining the solution to an inverse problem in conventional research [23]. If condition number of the transfer matrix is very large, the dipole source is very sensitive to the near-field data and the solution matrix would not be unique [24]. The dipole source stability can be improved by regularization algorithms that suppress the perturbation influence of the measurement error in near-field data.

Tikhonov regularization is standard for mitigating the ill conditioning of the inverse problem [25]. Both Tikhonov regularization and the conjugate gradient method are used to obtain a convergent solution as mentioned in [26]. The SVD method is not only useful for reducing the effect of ill conditioning, but also capable of ensuring the quality and sufficiency of the near-field data [27]. The regularization coefficient is used to adjust the weight of the stability and accuracy of the solution source matrix [28]. The regularization coefficient can be obtained by the diverse methods such as ''L-Carve'', intelligent optimization algorithm, generalized cross validation, machine learning and TSVD [29]–[31].

However, it is difficult to select a suitable regularization coefficient when the level of error is not clear and the transfer matrix has a large scale. In addition, the regularization iteration steps can be extremely time-consuming when the transfer matrix is very complex. The number of iteration steps increases when the regularization cannot converge rapidly.

Because of the unavoidable drawbacks in near-field phase measurement, some research on the phaseless scanning has become very interesting [32]–[34]. The main research is composed of the intelligent optimization method, the adjoint method and the phase angle gradient method. Based on these methods, the equivalent source model can be calculated with just the amplitude information.

In this paper, a new transfer model that can reflect the relationship between the dipole source (P_z, M_x and M_y) and electromagnetic field (E_z, H_x and H_y) is derived. Compared with the conventional transfer matrix, tangential component of electric field (E_x E_y) is replaced by the normal component of electric field (E_z). And the tangential component of magnetic field (H_x, H_y) is retained in the new transfer matrix. Therefore, the total measurement time of the near-field data can be decreased by 25%. And the computation time of dipole source can be substantially decreased because of the smaller size of the transfer matrix. Because the perturbation produced by normal component E-probe is smaller than the tangential component E-probe, the error in near-field data is reduced.

In this paper, an efficient regularization method is proposed to calculate a stable and accurate equivalent dipole source with the new transfer matrix. The new method is based on the cross-contrast between Tikhonov and TSVD mentioned in [25]. The final solution that can converge rapidly is obtained through an iterative comparison process. Based on region division, the new regularization method can be used to calculate the equivalent source of a large-scale problem. The evident advantages of the solution can be proven by simulation and measurement.

This paper is organized as follows: The descriptions of the new transfer model and inverse problem are introduced in Section II. In Section III, the proposed regularization algorithm is described in detail. The results of the numerical simulation and measurement are presented in Section IV to verify the validation of this approach, followed by conclusion in Section V.

II. NEW TRANSFER MODEL AND INVERSE PROBLEM

The main idea of the equivalent dipole model is based on the multipole expansion theory [36]. The radiation source can be replaced by a set of dipoles: electric dipoles denoted P_x, P_y and P_z, and magnetic dipoles denoted M_x, My and Mz. When the PCB signal plane is very close to a ground plane and the DUT is a microwave or high-speed digital circuit, the impact of the finite ground edge can be tolerated [37]. Notice that, only three dipoles P_z, M_x and M_y are enough to create the equivalent dipole array [16]. As shown in Fig.1, the electromagnetic field data of DUT is measured on the near-field scanning plane firstly. And then, the equivalent dipole source can be extracted with the scanning data and transfer matrix. Finally, the field distribution in the half space above the DUT can be obtained based on the equivalent source.

The electromagnetic fields generated by the dipole source above an infinite ground plane can be calculated analytically [38]. As shown in Fig.2, the electromagnetic field from z-polarized dipole at the origin of a spherical coordinate can

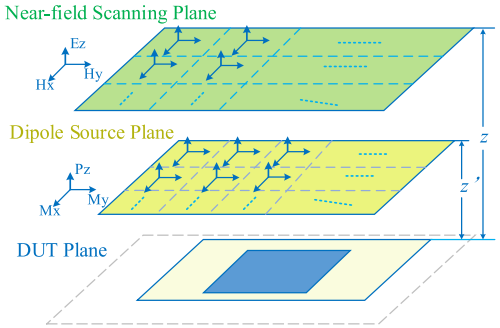

FIGURE 1. Equivalent dipole model based on near-field scanning.

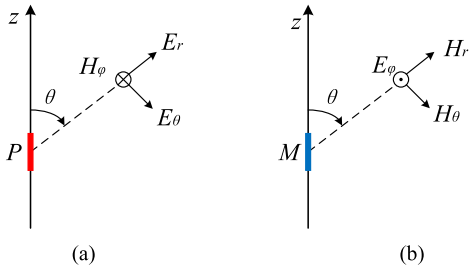

FIGURE 2. Electric dipole (a) and magnetic dipole (b).

be calculated as [39]

$$H_\varphi = \frac{jkI^eL}{4\pi r}\sin\theta(1+\frac{1}{jkr})e^{-jkr} \quad (1)$$

$$E_r = \frac{\eta I^eL}{2\pi r^2}\cos\theta(1+\frac{1}{jkr})e^{-jkr} \quad (2)$$

$$E_\theta = \frac{j\eta kI^eL}{4\pi r}\sin\theta(1+\frac{1}{jkr}-\frac{1}{k^2r^2})e^{-jkr} \quad (3)$$

$$E_\varphi = -\frac{jkI^mL}{4\pi r}\sin\theta(1+\frac{1}{jkr})e^{-jkr} \quad (4)$$

$$H_r = \frac{I^mL}{\eta\cdot 2\pi r^2}\cos\theta(1+\frac{1}{jkr})e^{-jkr} \quad (5)$$

$$H_\theta = \frac{jkI^mL}{\eta\cdot 4\pi r}\sin\theta(1+\frac{1}{jkr}-\frac{1}{k^2r^2})e^{-jkr} \quad (6)$$

where I_e and I_m are complex number denoting the electric current and magnetic current, k is the space wave number in vacuum, L is the length of dipole, η is wave impedance in free-space, and r is the distance from the measurement point to the dipole. The electromagnetic fields (F) excited by the equivalent dipole source (X) can be calculated as a matrix equation.

$$TX = F \quad (7)$$

where T is the transfer matrix that denotes the relationship between the electromagnetic field and dipole source. The spherical coordinates should be converted to rectangle coordinates, because of planar near-field scanning and planar distribution of dipoles. In previous research [16], the data vector F includes the tangential component of near-field distribution E_x, E_y, H_x and H_y. However, in this paper, vector F is composed of normal component of electric field E_z and tangential component of magnetic field H_x and H_y. The dipole solution vector X denotes the equivalent dipole source which includes P_z, M_x, and M_y. The electromagnetic fields at each observation points can be calculated as the linear superposition of the fields generated by all the dipole sources. Hence, equation (7) can be rewritten in two different forms.

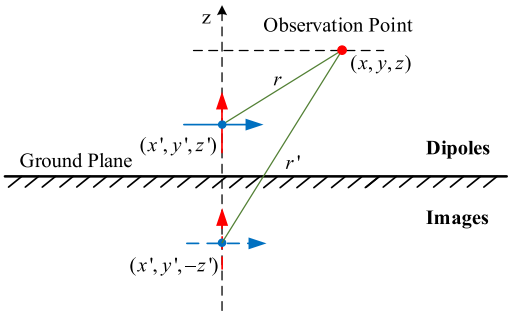

FIGURE 3. Image model of dipole source: Red arrow indicates electric dipole; Blued arrow indicates magnetic dipole.

$$\begin{pmatrix} T_{PzEx} & T_{MxEx} & T_{MyEx} \\ T_{PzEy} & T_{MxEy} & T_{MyEy} \\ T_{PzHx} & T_{MxHx} & T_{MyHx} \\ T_{PzHy} & T_{MxHy} & T_{MyHy} \end{pmatrix} \begin{pmatrix} P_z \\ M_x \\ M_y \end{pmatrix} = \begin{pmatrix} E_x \\ E_y \\ H_x \\ H_y \end{pmatrix} \quad (8)$$

$$\begin{pmatrix} T_{PzEz} & T_{MxEz} & T_{MyEz} \\ T_{PzHx} & T_{MxHx} & T_{MyHx} \\ T_{PzHy} & T_{MxHy} & T_{MyHx} \end{pmatrix} \begin{pmatrix} P_z \\ M_x \\ M_y \end{pmatrix} = \begin{pmatrix} E_z \\ H_x \\ H_y \end{pmatrix} \quad (9)$$

where the conventional and new proposed transfer matrices are presented as (8) and (9) respectively. And it is obvious that the new transfer model needs fewer near-field data, and the scale of transfer matrix is also reduced. It is helpful to improve the efficiency of solving such an inverse problem in both computation and storage. The number of test points over near-field scanning plane is set as $M \times M$. The dimensions of submatrix in F are $M^2 \times 1$. The number of each kind of dipole is assumed to be $N \times N$, the dimensions of submatrix in X should be $N^2 \times 1$.

The submatrix of T indicates the relationship between electromagnetic fields and dipoles. As shown in Fig.3, the field distribution can be calculated as the superposition of field created by the dipoles and their images. Therefore, the detailed expressions of T_{PzEz}, T_{MxEz}, T_{MyEz} T_{PzHx}, T_{MxHx}, T_{MyHx}, T_{PzHy}, T_{MxHy} and T_{MyHy} are given as (10) - (18). To simplify the equations, the expansions of terms $f_1(d)$ and $f_2(d)$ are given as (19) and (20), respectively.

$$T_{PzEz} = \frac{\eta}{2\pi}[\frac{f_1(r)(z-z')^2}{r^3} + \frac{f_1(r')(z+z')^2}{(r')^3} - \frac{jk((x-x')^2+(y-y')^2)}{2}(\frac{f_2(r)}{r^2}+\frac{f_2(r')}{(r')^2})] \quad (10)$$

$$T_{MxEz} = \frac{-jk}{4\pi}[\frac{f_1(r)(y-y')}{r} + \frac{f_1(r')(y-y')}{r'}] \quad (11)$$

$$T_{MyEz} = \frac{jk}{4\pi}[\frac{f_1(r)(x-x')}{r} + \frac{f_1(r')(x-x')}{r'}] \quad (12)$$

$$T_{PzHx} = -\frac{jk}{4\pi}\cdot\left(\frac{f_1(r)}{r^2}+\frac{f_1(r')}{(r')^2}\right)\cdot(y-y') \tag{13}$$

$$\begin{aligned} T_{MxHx} = {} & \frac{1}{2\pi\eta}\frac{(x-x')(y-y')}{[(x-x')^2+(y-y')^2]^{1/2}}\left[\frac{(z-z')f_1(r)}{r^4}\right. \\ & \left.+\frac{(z+z')f_1(r')}{(r')^4}\right]+\frac{jk}{4\pi\eta}\frac{y-y'}{[(x-x')^2+(y-y')^2]^{1/2}} \\ & \left[\frac{[(x-x')^2+(z-z')^2]^{1/2}(z-z')f_2(r)}{r^3}\right. \\ & \left.+\frac{[(x-x')^2+(z+z')^2]^{1/2}(z+z')f_2(r')}{(r')^3}\right] \end{aligned} \tag{14}$$

$$\begin{aligned} T_{MyHx} = {} & \frac{1}{2\pi\eta}\frac{(x-x')^2}{[(x-x')^2+(y-y')^2]^{1/2}}\left[\frac{(z-z')f_1(r)}{r^4}\right. \\ & \left.+\frac{(z+z')f_1(r')}{(r')^4}\right]+\frac{jk}{4\pi\eta}\frac{(y-y')}{[(x-x')^2+(y-y')^2]^{1/2}} \\ & \left[\frac{[(y-y')^2+(z-z')^2]^{1/2}(z-z')f_2(r)}{r^3}\right. \\ & \left.+\frac{[(y-y')^2+(z+z')^2]^{1/2}(z+z')f_2(r')}{(r')^3}\right] \end{aligned} \tag{15}$$

$$T_{PzHy} = \frac{jk}{4\pi}\cdot\left(\frac{f_1(r)}{r^2}+\frac{f_1(r')}{(r')^2}\right)\cdot(x-x') \tag{16}$$

$$\begin{aligned} T_{MxHy} = {} & \frac{1}{2\pi\eta}\frac{(y-y')^2}{[(x-x')^2+(y-y')^2]^{1/2}}\left[\frac{(z-z')f_1(r)}{r^4}\right. \\ & \left.+\frac{(z+z')f_1(r')}{(r')^4}\right]-\frac{jk}{4\pi\eta}\frac{(x-x')}{[(x-x')^2+(y-y')^2]^{1/2}} \\ & \left[\frac{[(x-x')^2+(z-z')^2]^{1/2}(z-z')f_2(r)}{r^3}\right. \\ & \left.+\frac{[(x-x')^2+(z+z')^2]^{1/2}(z+z')f_2(r')}{(r')^3}\right] \end{aligned} \tag{17}$$

$$\begin{aligned} T_{MyHy} = {} & \frac{1}{2\pi\eta}\frac{(x-x')(y-y')}{[(x-x')^2+(y-y')^2]^{1/2}}\left[\frac{(z-z')f_1(r)}{r^4}\right. \\ & \left.+\frac{(z+z')f_1(r')}{(r')^4}\right]-\frac{jk}{4\pi\eta}\frac{(x-x')}{[(x-x')^2+(y-y')^2]^{1/2}} \\ & \left[\frac{[(y-y')^2+(z-z')^2]^{1/2}(z-z')f_2(r)}{r^3}\right. \\ & \left.+\frac{[(y-y')^2+(z+z')^2]^{1/2}(z+z')f_2(r')}{(r')^3}\right] \end{aligned} \tag{18}$$

$$f_1(d) = \left(1+\frac{1}{jkd}\right)\frac{e^{-jkd}}{d} \quad (d = r, r') \tag{19}$$

$$f_2(d) = \left(1+\frac{1}{jkd}-\frac{1}{k^2d^2}\right)\frac{e^{-jkd}}{d} \quad (d = r, r') \tag{20}$$

where x, y and z denote the coordinates of the test points and x', y' and z' denote the locations of the dipole array. The terms r and r' which can be calculated as (21) and (22) are the distances from the test points to the three dipoles and their images.

$$r = [(x-x')^2+(y-y')^2+(z-z')^2]^{1/2} \tag{21}$$

$$r' = [(x-x')^2+(y-y')^2+(z+z')^2]^{1/2} \tag{22}$$

There are two simulation examples used to illustrate the difference between the old transfer matrix and the new transfer matrix. In the first example, the height of near-field scanning plane is set as 3 mm and the height of dipole plane is set as 0.25 mm. The simulation frequency is 2 GHz. The interval between the test points and the dipoles is 1 mm, respectively. The sample points and dipoles are distributed uniformly over the two planes. The condition numbers of the conventional transfer matrix (*Con.*) and the new transfer matrix (*New.*), and the computation times and cache memories of the different programs are presented in Table 1. It is obvious that the condition number of new transfer matrix is more stable and the new transfer model is more efficient with increasing of matrix scale.

TABLE 1. Comparison between two transfer matrices.

Number Of M/N	Condition Number		Computation Time(s)		Cache Memory (MB)	
M/N	*Con.*	*New.*	*Con.*	*New*	*Con.*	*New*
21/21	2.6E3	1.3E3	4.3	3.2	125.7	99.3
41/41	4.3E3	1.3E3	48.6	39.9	1824.1	1510.1
61/61	5.8E3	1.3E3	416.2	313.5	4939.2	3992.7

TABLE 2. Error of fields calculated by different matrices (%).

Index	M/N	*Ex*	*Ey*	*Ez*	*Hx*	*Hy*	*Hz*
T_o	21/21	1.81	1.82	9.44	2.14	2.23	8.65
T_o	41/41	1.50	1.52	9.17	2.03	2.09	8.17
T_n	21/21	4.42	5.32	1.54	2.18	2.24	7.33
T_n	41/41	3.96	4.21	1.12	2.06	2.08	6.56

In the second example, the numbers of test points and dipoles are given as M and N. The height of the observation plane is set as 2 mm and the height of dipole array is set as 1 mm. The simulation frequency is set as 1GHz. The equivalent source is determined based on the old matrix and new matrix with same regularization method, respectively. And the relative errors of all components are given in Table 2. Due to the decrease of near-field data, the error of H_x and H_y calculated based on the new matrix may increase by about 0.4% compared with the old matrix. Both the old matrix and new matrix may result in a large error in calculation of H_z. The old matrix (T_o) has better performance in calculation of E_x and E_y. The new matrix (T_n) has an evident advantage in calculation of E_z.

The equivalent dipole solution X is obtained with near-field data F and transfer matrix T. It is a typical inverse problem for calculating a dipole matrix. If the transfer matrix T is well-condition, the dipole solution could be calculated with the least square method. However, T is often an ill-posed matrix in the EMC problems, which means the stability and accuracy of solution X is potentially sensitive to the perturbation in the near-field data F. Because of the inevitable errors caused by

measurement and computer truncation, equation (7) can be written as

$$(\hat{T} + E_T) \cdot (\hat{X} + E_X) = (\hat{F} + E_F) \tag{23}$$

where matrix F denotes the actual near-field data without error E_F. Matrix T denotes the original transfer matrix without error E_T. Matrix X indicates the stable dipole matrix, E_X is the error caused by the perturbation included in T and F. And the relative error of the solution matrix can be derived as equation (24).

$$\frac{\|E_X\|}{\|X\|} \leq \frac{\|T\| \cdot \left\|T^{-1}\right\|}{1 - \|T\| \cdot \left\|T^{-1}\right\| \frac{\|E_T\|}{\|T\|}} \left(\frac{\|E_T\|}{\|T\|} + \frac{\|E_F\|}{\|F\|}\right) \tag{24}$$

The $\|\cdot\|$ denotes the Euclidean norm of matrix, and $cond(T) = \|T\| \cdot \|T^{-1}\|$ is defined as the condition number of transfer matrix T. The form $\|E_A\|/\|A\|$ denotes the relative error of matrix A. Equation (24) can be rewritten as the following when the error of T is very small and can be ignored.

$$\frac{\|E_X\|}{\|X\|} \leq cond(T) \cdot \frac{\|E_F\|}{\|F\|} \tag{25}$$

It is obvious that the relative error of dipole solution is mainly affected by the error in F. To improve the accuracy of dipole solution, the condition number of T is supposed to be reduced. Therefore, a suitable regularization method should be used in solving such an inverse problem.

III. CONDITION NUMBER AND REGULARIZATION

As discussed earlier, it indicates that the stability and accuracy of the solution matrix are mainly impacted by the condition number of transfer matrix and the relative error of near-field scanning data. In order to improve the dipole source solution, the condition number should be reduced to avoid amplifying the upper limit of error E_x. This reduction is very important for the further research of equivalent dipole model based on a well-conditioned transfer matrix.

A. OPTIMIZED CONDITION NUMBER

Previous work [22] has payed attention to factors which can influence the condition number of transfer matrix. If the total number of test points is set as a constant value, the number of dipoles, the interval of dipoles and the distribution of the dipoles drastically impact the condition number,

To locate the real noise source accurately, the distance between the measurement plane and surface of DUT should be very small, and the interval between two closed test points should be as small as the spatial resolution of near-field probe. High-resolution scanning is necessary in EMI diagnosis of PCB. To represent the electromagnetic field distribution of DUT, it is better to select a high-density dipole array. However, a large number of the measurement points and dipoles are time consuming and result in a large condition number of the transfer matrix. A suitable transfer matrix can be selected based on following steps;

1) To reconstruct the dipole source accurately and efficiently, the number of measurement points (M) and number of dipoles (N) should be suitable. There is no quantitative relation between M and N. A comparison simulation result given in Table 3 is used to illustrate the relative error of the dipole source with different selection of M and N. The heights of near-field observation plane and dipole plane keep unchanged. And the observation area is equal to the dipole area. As given in Table 3, with the increase of N, the relative error decreases firstly. And then, the relative error changes unobvious. Finally, the relative error increase. It indicates that the difference between M and N should not be too large or too small to avoid large relative error in engineering application.

TABLE 3. Relative error of dipole source with different M and N(%).

M \ N	3	5	7	9	11	13	15	17	19	21
13	12.7	8.5	2.7	1.8	1.3	1.3	1.5	1.4	2.1	3.5
M \ N	20	21	22	23	24	25	26	27	28	29
25	9.6	7.2	4.5	2.1	1.6	1.5	1.5	1.4	3.5	4.8
M \ N	30	31	32	33	34	35	36	37	38	39
37	16.3	12.2	7.8	3.2	1.9	2.1	2.3	2.2	2.6	6.9

2) The interval between two closed dipoles can be same or not to adapt the different models. When the DUT is large or homogeneous, the locations of dipoles should be uniform to enhance the efficiency. And if the DUT is specific or anisotropic, the interval of the dipoles can be different and more dipoles can be placed in the interest area;

3) The distribution area of the dipoles should not be too small to avoid an undesired dipole solution. And the dipole area should increase when the distance between the scanning plane and the dipole array plane decreases. Otherwise, the serious errors will appear at the edges of observation area;

To research the change of condition number of different transfer matrixes, some numerical experiments results are obtained and presented. The main steps of the experiments are given as follows. Firstly, the location of the test point is provided. And then, the dipole array is designed, the range of the dipole number, the alternative value of the dipole interval and the distribution area are determined in this step. Finally, the condition number of the transfer matrix is calculated. In this paper, an accelerated iteration method is used in optimizing the transfer matrix.

The transfer matrix is built as a multiport model in MATLAB. The types of input variables include N_T (number of test points), N_D (number of dipoles), L_T (coordinates of test points), L_D (coordinates of dipoles), H_T (height of near-field scanning plane), H_D (height of dipole array plane), and f (simulation frequency). The output variable is C_T (condition number of transfer matrix). These input variables are initialized at beginning of the accelerated algorithm, and changed at each iteration. The accelerated method is based on the gradient change of C_T with different input variables. The variations of input variables will automatically decrease when

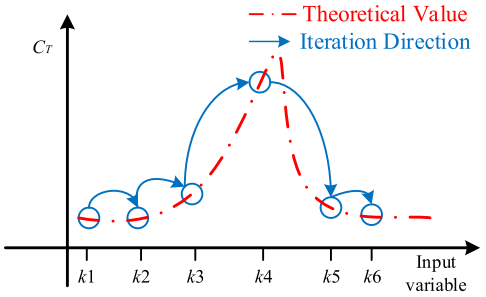

FIGURE 4. The accelerated iteration method.

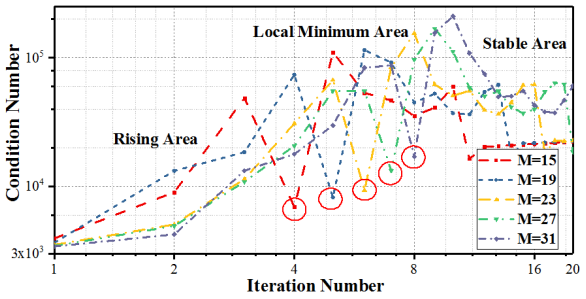

FIGURE 5. The condition number calculated with different iteration numbers.

the change of C_T is drastic. This is helpful for improving the performance of transfer matrix selection in both computing time and accuracy. As shown in Fig.4, the different values k_i $(i = 1, 2, \ldots)$ of input variables are used to calculate C_T. The gradient value of C_T at k_1 is recorded and compared with the one at k_2. If the change of gradient became smaller, the interval between k_2 and k_3 would enlarge automatically. In the contrast, the step interval will decrease when the gradient has changed larger. If the gradient changes sign at several sample points, the condition number is close to the locally optimal solution and the iteration stops at the minimum sample point. And the minimum interval and maximum iteration number will be set to avoid a great number of computations.

This method can be used to analyze the influence of each input variable mentioned earlier, and ultimately select a suitable transfer matrix. It is always an efficient method to calculate the transfer matrix when the test points and dipoles are distributed uniformly on the observation plane and dipole plane. Where the variations of N_T and T_D are positive integer and no less than 1. The number $(M \times M)$ of test points on the near-field scanning plane indicates that there are M test points in both x and y direction. For this example, the distribution of near-field scanning points is uniform, and the interval between two adjacent observation points is 1 mm. The maximum interval can reach to one-tenth of the wavelength. The minimum interval is subject to the spatial resolution of near-field probe. Firstly, the height z of scanning plane is 2 mm, and the height z' of dipole plane is1mm. Moreover, the number of dipoles is set as $N \times N$. As for different DUT, the minimum of N is selected as $(M\text{-}1)/2 + 2^*I$ (I: Iteration number, $I = 1, 2\cdots$). The upper limit of N is determined by the iteration algorithm. The maximum iteration number is set as 20. A numerical result is presented in Fig.5.

When the iteration number is less than approximately $M/4$, the condition number is monotone increasing. And it is obvious that the change in the condition number is more dramatic with the increasing iteration number. When $I = (M + 1)/4$, the condition number is a local minimum point. The change is alleviated when $I > M/4+5.25$. This conclusion is helpful for selecting a suitable transfer model. However, the computation time of dipole solution still increases quickly when the DUT has a large size. Thus, the research into the efficiency and accuracy of the solution becomes more attractive. A proposed regularization technique is given as follows.

B. REGULARIZATION TECHNIQUE

The transfer matrix should be optimized to obtain a suitable condition number which determines the relative error upper-limitation of the dipole solution. It is helpful to obtain a suitable equivalent solution with regularization. To solve the ill-posed inverse problem such as (23), two widely used regularization methods mentioned in previous work are Tikhonov regularization and TSVD [25]. The characteristics of the two methods are different.

To obtain a stable and accurate equivalent dipole source, the objective function of Tikhonov is defined as

$$R_C = \min_{X \in R}\{\|TX - F\|^2 + \mu^2 \|X\|^2\} \tag{26}$$

The regularization coefficient μ is a positive number, and used to balance the weights of $\|TX - F\|^2$ and $\|X\|^2$. The first term presents the accuracy of vector X, and the second term impact the stability of the equivalent solution. The regularization solution of (26) is expressed as

$$X_\mu = [T^T T + \mu^2 I]^{-1} \cdot T^T F \tag{27}$$

where I is an identity matrix and the superscript T denotes the matrix transposition. A suitable μ determines how accurate and stable the dipole solution matrix is. Commonly used methods for selecting μ include "L-curve", discrepancy principle, the quasi-optimality principle and Generalized cross validation. However, this regularization has not been analytically proven to be absolutely convergent. And the methods based on the discrepancy principle would be invalid when the level of error in the near-field data is unavailable.

Singular value decomposition (SVD) is a popular method for dealing with the matrix operation [27]. The SVD form of transfer matrix T can be written as

$$T = UAV^T \tag{28}$$

where the matrices

$$U = [u_1, u_2, \cdots, u_{3M^2}]_{3M^2 \times 3M^2} \tag{29}$$

$$V = [v_1, v_2, \cdots, v_{3N^2}]_{3N^2 \times 3N^2} \tag{30}$$

$$A = \begin{pmatrix} A_r & 0 \\ 0 & 0 \end{pmatrix}_{3M^2 \times 3N^2} \tag{31}$$

$$A_r = diag[\sigma_1, \sigma_2, \cdots, \sigma_r]_{r \times r} \tag{32}$$

where the unitary matrices U and V are composed of column vectors u_i and v_i. Where the diagonal matrix A_r consists of the positive singular values of T. The subscript r denotes the number of positive singular values (in other words, the rank of T). And they are ordered as $\sigma_1 \geq \sigma_2 \geq \ldots \geq \sigma_r > 0$. According to (28)-(32), the Moore-Penrose solution X can be written as

$$X_k = \sum_{i=1}^{k} \frac{v_i u_i^T}{\sigma_i} F \tag{33}$$

where k is the number of singular values left in TSVD. And the last r-k diagonal elements of A_r are removed, because that the error in the near-field data can significantly affect the dipole solution when the singular values are small. It is obvious that $\|X_k\|$ increase and $\|F\text{-}TX_k\|$ decrease monotonically with the increase of k. However, the change in solution X_k is not continuous.

Numerous numerical experiments suggest that the regularization solution X_μ should be approximate to the TSVD solution X_k for the same model. However, the parameter μ can change continuously in the domain of definition, and k is an integer range from 1 to r. The calculation of X_μ will take a lot of time but the solution has a higher accuracy. X_k can be computed completely in several iterations, but may be not the optimal solution.

The accuracy and efficiency of the solution are impacted by both k and μ. According to the Moore-Penrose solution (33) for an equivalent source, the regularization solution (27) can be calculated as

$$X_{\mu k} = \sum_{i=1}^{k} \frac{\sigma_i \cdot v_i u_i^T}{\sigma_i^2 + \mu^2} F \tag{34}$$

The truncation factor $\delta_i = \sigma_i/(\sigma_i^2+\mu^2)$ is decrease with the increasing of i. To determine the value of k, the factor δ_i can be assumed as zero when δ_i is less than a known condition. Then, the regularization solution X_{uk} is obtained.

The process of the proposed regularization method is presented in Fig.6.

1) Obtain the singular value of transfer matrix T, and record the unitary matrix and diagonal matrix;

2) Calculate a rough regularization coefficient μ with L-curve method;

3) Compute the truncation factor $\delta_i = \sigma_i/(\sigma_i^2 + \mu^2)$. If δ_i is less than a convergence condition such as 10^{-3}, the last r-i diagonal elements of A_r are removed. The parameter k should be i-1;

4) According to 1), 2) and 3), the optimized solution can be calculated by (33).

It is an effective method to calculate such an inverse problem, because that the dimension of the original transfer matrix can be reduced automatically when the convergence condition is satisfied. The compute efficiency can increase exponentially.

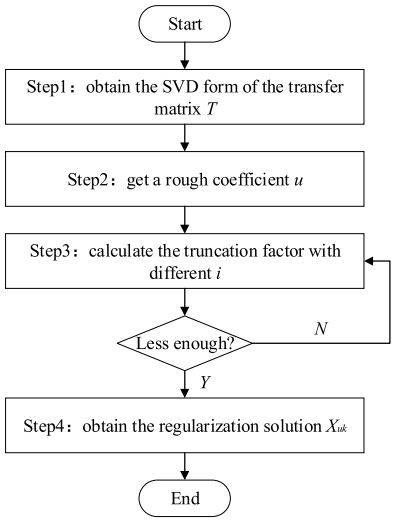

FIGURE 6. Flow chart of the proposed regularization method.

TABLE 4. The detailed information of probes.

	Probes	Work Band	Maximum Size(mm)	Spatial Resolution
1	E-Probe[41]	9kHz-40GHz	15×48	1mm
2	H-Probe[1]	9kHz-10GHz	15×48	1mm

IV. VALIDATION AND DISCUSSION

In this section, the detailed application procedure of the equivalent dipoles source is introduced firstly. And there are five examples based on simulation and measurement to verify the validation of new transfer model and new regularization method.

A. INTRODUCTION OF DIPOLE SOURCE APPLICATION

In this part, the whole extraction procedure of the equivalent dipole source is introduced. The flowchart is presented in Fig.7. Firstly, the near-field data of electric device is measured by near-field probes. And then, the transfer matrix is determined based on the main steps mentioned in Section II-A. Meanwhile, the equivalent dipole source is calculated based on the proposed regularization method. Finally, the equivalent source can be used to calculate the field distribution in any observation points.

There are some specific requirements of the near-field probes mentioned in step 1. (1) The work band of probe should cover the near-field measurement frequency. (2) And the size of probe should be small enough to measure the field distribution in narrow and complex space. (3) The spatial resolution should be small enough to meet the need of high-resolution near-field scanning. The detailed information of the near-field probes used in step 1 is given in Table 4.

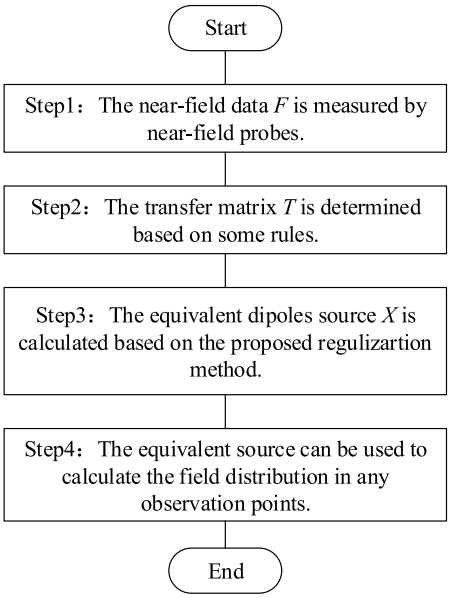

FIGURE 7. Typical flowchart of the equivalent source extraction.

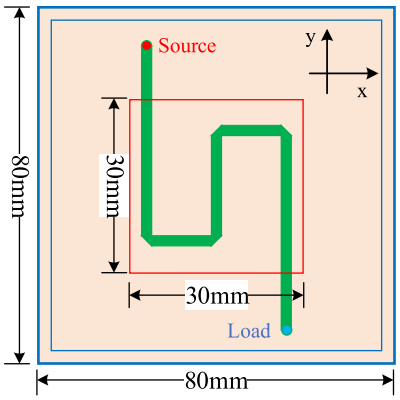

FIGURE 8. The simulation area (red line) of delay line in CST.

In addition, the near-field probes are calibrated by the professional institute (China Aerospace Science and Industry Corporation, 203 Laboratory). The calibrated process is carried out based on the IEEE standard [40].

B. SIMULATION OF DELAY LINE

The proposed equivalent dipole source and regularization method is validated with a simulation model as shown in Fig.8. The dimension of the PCB is 80mm × 80mm. The trace is 1oz thick and 1mm above the ground plane. The signal trace is driven by a single frequency source and terminated by a load of 50Ω. The near-field data of the selected area are obtained on a plane which is 4mm above the ground plane. And the total number of observation points is 31 × 31. The normal component of electric field and tangential component of magnetic field are simulated and presented in Fig.8.

As discussed earlier, the stability and accuracy of the solution matrix are impacted by both the condition number of the transfer matrix and the noise level of the near-field

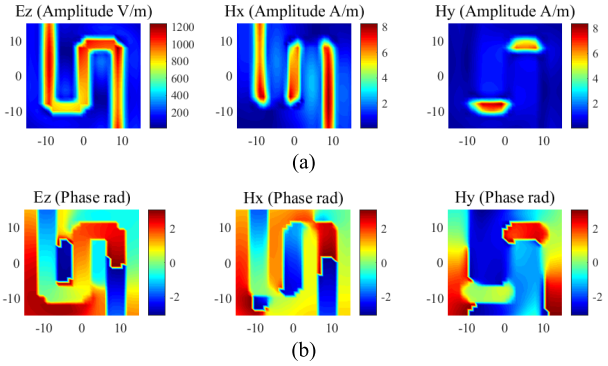

FIGURE 9. The simulation field data: (a) The amplitude distribution (b) The phase distribution.

TABLE 5. Relative errors of different methods.

Results	Tikhonov	TSVD	New Method
Error	1.6%	3.2%	0.87%

scanning data. The distribution of dipoles is determined based on the work mentioned in Section II. There are 31 × 31 dipoles uniformly distributed on the dipole plane. The height of dipole plane is 3.5 mm and the interval between two closed dipoles is 1 mm. The distribution of the electromagnetic field on the observation plane shown in Fig.9 is calculated with the proposed regularization method.

To quantify the validation of the regularization method, the relative error between the numerical result and the reference result is defined as

$$Error = \frac{1}{M} \cdot \sum_{i,j=1}^{M} \frac{\|F_{sim}(i,j) - F_{cal}(i,j)\|}{\|F_{sim}(i,j)\|} \tag{35}$$

where (i, j) denotes the index of observation points, M is the number of test points. For this model, the relative errors of different regularization methods are given in Table 5. The equivalent dipole solution is built and simulated as a radiation source in MATLAB. The amplitude information can be obtained from X and the initial phase is set as zero. The tangential components of the electric field from the original structure and from the equivalent simulation model are compared in Fig.10.

The dipole solution can be described as a linear model

$$X = f(K, L_o, L_D, E_z, H_x, H_y) \tag{36}$$

where f is a function signature depending on the flowing constraint conditions. K is a constant coefficient. L_o and L_D are the locations of the near-field scanning point and dipole respectively. E_z, H_x and H_y are the near-field data composed of amplitude and phase. For a singular matrix, the solution will be more accuracy with more constraint conditions. In other word, the range of solution is lager when the constraint conditions are not sufficient. The tangential component of the electric field can be calculated and simulated by the equivalent dipole model. However, the difference

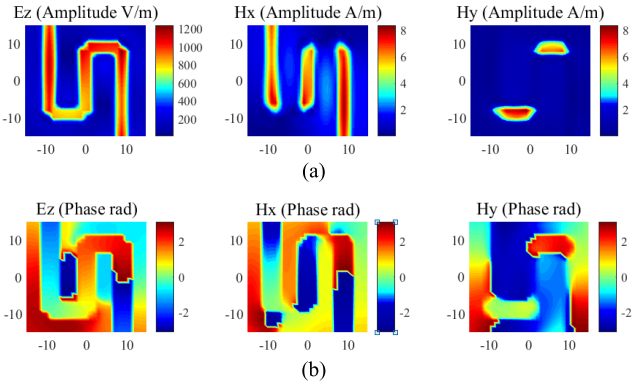

FIGURE 10. The calculated result data: (a) The amplitude distribution (b) The phase distribution.

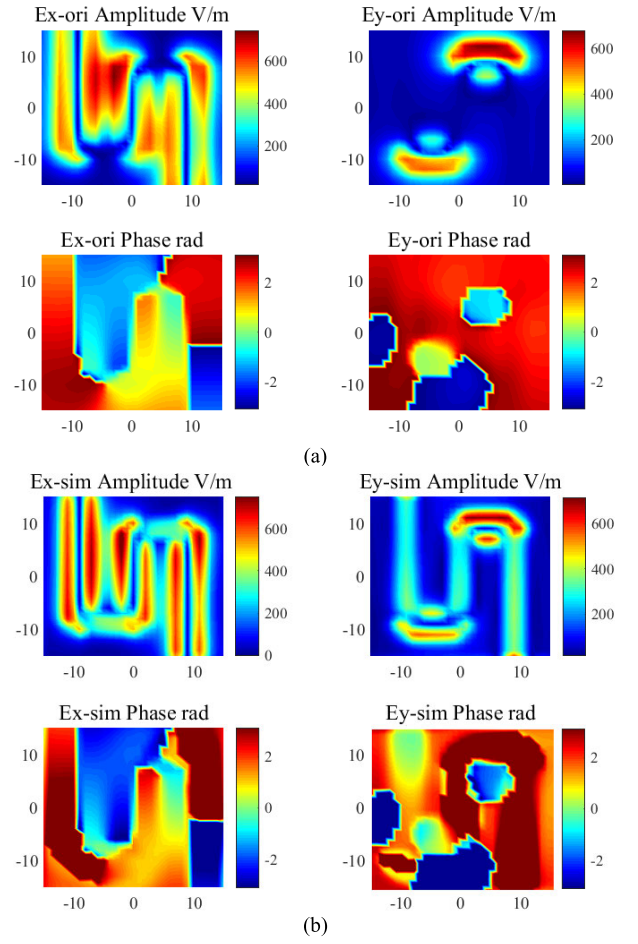

FIGURE 11. The tangential component of electric field: (a) The field from original structure (b) The field from equivalent dipole model.

in Fig.11 is inevitable. And the maximum relative error is less than 5.3%.

C. APPLICATION IN MICROSTRIP ANTENNA

In this part, a microstrip antenna is used as a DUT to verify the proposed research. The microstrip antenna model is given in Fig.12. The dimension of the ground plane is

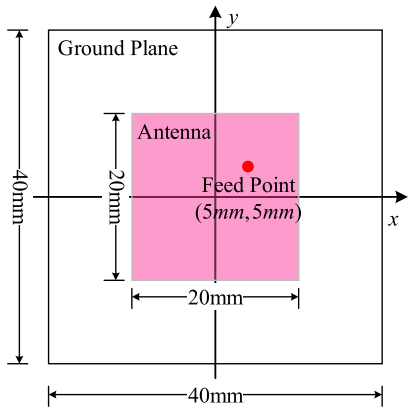

FIGURE 12. The microstrip antenna model.

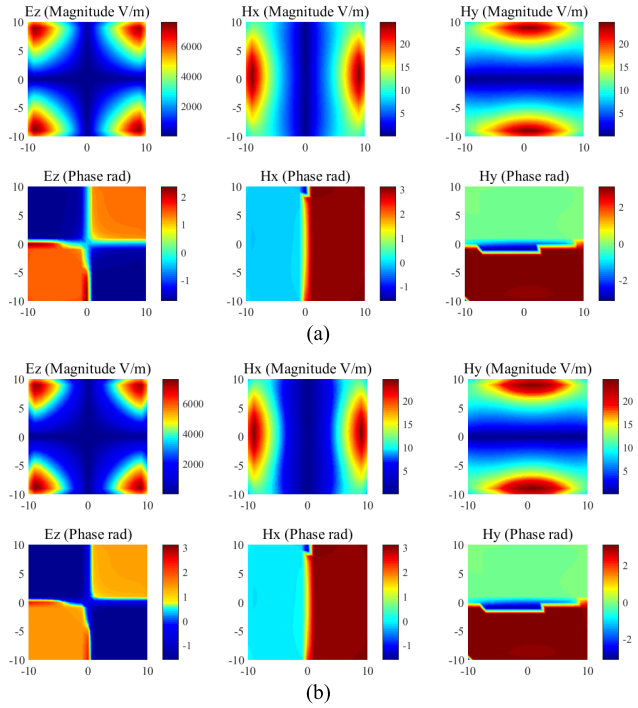

FIGURE 13. The near-field distribution of the microstrip antenna: (a) Simulation model (b) Dipole source.

40mm × 40mm, and the dimension of the microstrip antenna is 20mm × 20mm. The dielectric material is FR4, and the thickness of the dielectric material is 1mm. The antenna model is built and simulated in full wave tool HFSS. The feed point is set at (5mm, 5mm), and the simulation frequency is set as 7.5GHz. The height of near-field observation plane is set 3mm, the height of dipole array plane is set as 2mm. The number of near-field observation points is 21 × 21, and the number of dipoles is set as 31 × 31.

The field distribution on the near-field observation plane is presented in Fig.13(a). The field distribution calculated by the equivalent dipole source is given in Fig.13(b). The comparison results of the radiation pattern in plane XoY are given in Fig.14.

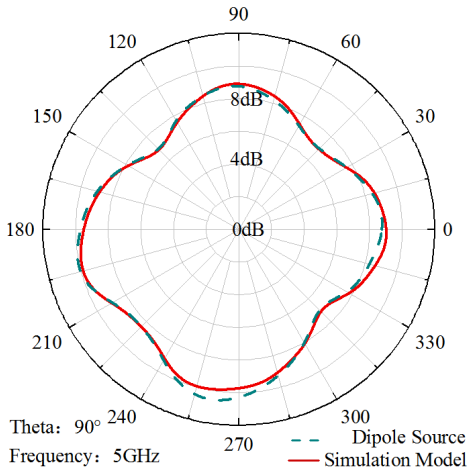

FIGURE 14. The antenna pattern results created by dipole source and simulation model.

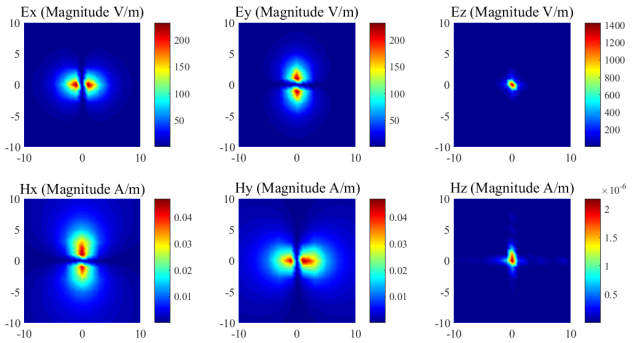

FIGURE 15. The EH-field distribution of an electric dipole.

TABLE 6. Relative errors of different methods.

Results	Tikhonov	TSVD	New Method
Near-field	3.65%	5.14%	1.62%
Radiation Pattern	4.54%	7.32%	1.39%

To illustrate the advantage of the proposed equivalent dipole source and the regularization method, the relation errors of near-field distribution and radiation pattern are given in Table 6. It is obvious that the near-field calculated by the dipole source fits well with the real near-field created by the antenna. And the relative error in the result based on the proposed regularization method is better than other two methods.

D. APPLICATION IN LARGE SCALE PROBLEM

As mentioned in [25], only Tikhonov is applicable in (even moderately) large scale problems. The proposed regularization process is time-consuming when the numbers of the test points and dipoles are very large. To improve the performance of the method in engineering applications. It is better to

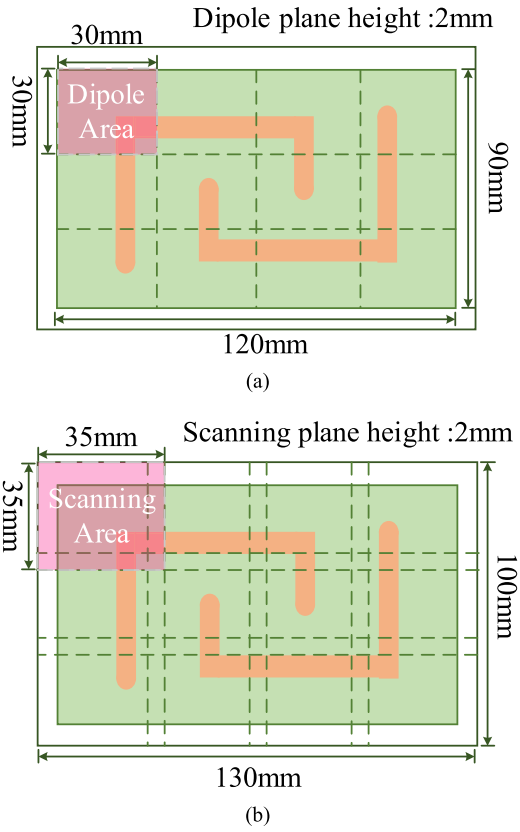

FIGURE 16. The divisions of a large size DUT: (a) Dimension of dipole subdomain (b) Dimension of near-field scanning subdomain.

divide the DUT into small size parts and compute these dipole source concurrently. Finally, the radiation pattern of DUT can be calculated by an assembled dipole source.

As given in (1)-(6), the E-/H- field strength decreases rapidly with the increase of r. Therefore, most electromagnetic energy exists near the dipole. To illustrate the field distribution clearly, a simulation result is presented in Fig.15. The height of the near-field scanning plane is 2mm. It is clear that the electromagnetic energy is very small when the distance between observation point and dipole is larger than 5mm. In this case, it is enough to calculate the equivalent source when the near-field scanning area is bigger than the dipole area about 5mm in x and y direction.

As shown in Fig.16, a large size DUT is divided into twelve parts and the whole scanning area is also divided into twelve parts. Each near-field scanning is bigger than the dipole array area. The twelve equivalent dipole solutions are calculated simultaneously firstly. And then, the dipole sources will be assembled as a whole dipole source. Finally, the radiation emission can be estimated by this equivalent source.

The size of the DUT is 120mm × 90mm, each dipole array area is 30mm × 30mm. The whole near-field scanning area is 130mm × 100mm, and each scanning area has a size of 35mm × 35mm. A full wave model is built and simulated in CST. And then the near-field data is divided into twelve matrices in Matlab. Each area has a same transfer

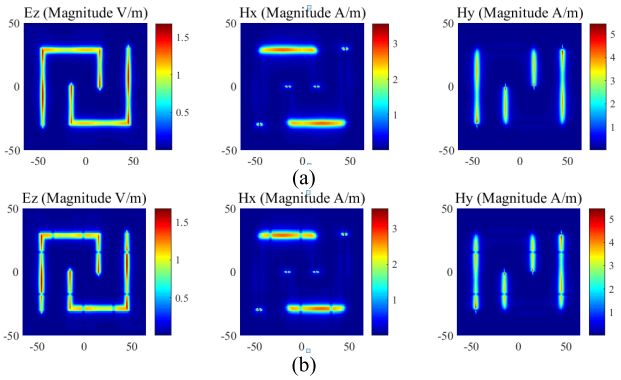

FIGURE 17. (a) Simulation results of PCB (b) Calculation results of equivalent dipole source.

TABLE 7. Relative errors of different methods.

Methods	Tikhonov	TSVD	New Method
Error	3.93%	5.12%	2.64%

matrix under this case. The comparison results between the calculation and simulation are given in Fig.17. The relation errors of near-field distribution based on different regularization method are given in Table 7. The new matrix and regularization method can be used to solve such a problem when the DUT has a large size.

In large scale problems, the size of subdomain should be neither too large nor too small. The calculation time of dipoles source will increase when the size of the subdomain is too large. Other process time will increase when the size of the subdomain is too small. Therefore, the size of each subdomain should be less than 40mm × 40mm. If the computer has a higher performance, the subdomain size could be larger.

E. APPLICATION IN COMPLEX ELECTRIC CIRCUIT

In this part, the motherboard of an intermediate frequency digitizer is used as the DUT to verify the proposed equivalent dipole model and regularization method. The photograph of the motherboard and near-field scanning area are shown in Fig.18. The dimension of the near-field scanning area is set as 30mm × 30mm. And the height of the scanning area is 4mm, the interval between two closed test points is 1mm. The amount of the test points is 31 × 31. The dipoles source plane is set as 2mm. The number of the dipoles is 25 × 25, and the interval between two closed dipoles is 1.25mm. The main steps of the whole process are given as following:

(1) The near-field data F shown in Fig.19 (a) is obtained.

(2) The transfer matrix T is determined as mention above.

(3) The equivalent dipole source X is calculated by the transfer matrix T and near-field data F.

(4) The field-distribution F_C calculated by dipole source is given in Fig.19 (b).

(5) The error between F and F_C is calculated and provided in Table 8.

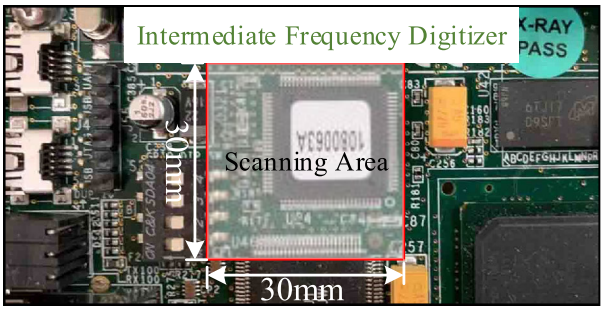

FIGURE 18. The photograph of the intermediate frequency digitizer motherboard.

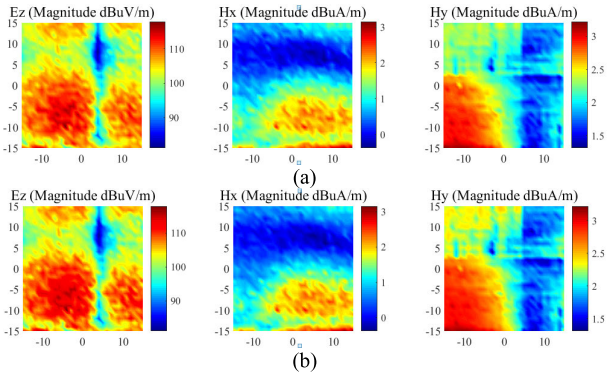

FIGURE 19. (a) Field distribution of the DUT (b) Calculation results of equivalent dipole source.

TABLE 8. Relative errors of different methods.

Methods	Tikhonov	TSVD	New Method
Error	2.98%	4.37%	1.55%

F. MEASUREMENT OF ENGINEERING PCB

As mentioned above, the simulation examples are designed to illustrate the validation of proposed regularization method and the effectiveness of new equivalent dipole extraction process. For any engineering PCB, the setting of near-field plane is introduced firstly. The heights of different components placed on the PCB should be considered. The minimum distance between the scanning plane and PCB should be large than the maximum height of electric components. In addition, the interval between two closed test points should be small enough to locate the noise source.

A simulation example is used to illustrate the importance of high-resolution scanning. There are nine electric dipoles used as the DUT. The height of near-field scanning plane is set as 4mm. The field distributions (Ez) at 350MHz with different scanning interval (K = 1, 2, 3 and 4mm) are presented in Fig. 20. It is obvious that the real emission source can be located accurately when the scanning interval is very small. Therefore, the high-resolution is very useful in engineering applications.

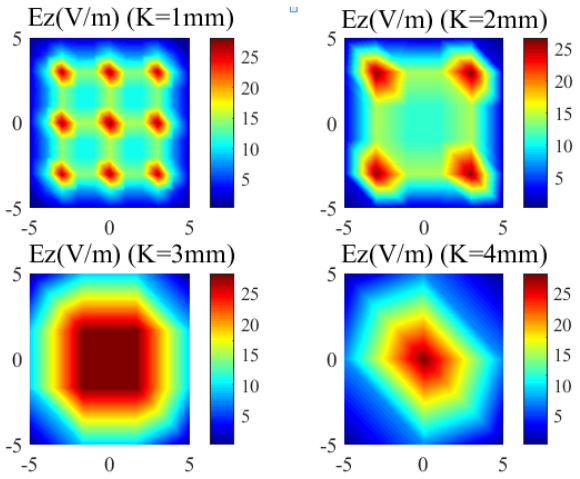

FIGURE 20. The distribution of Ez with different intervals.

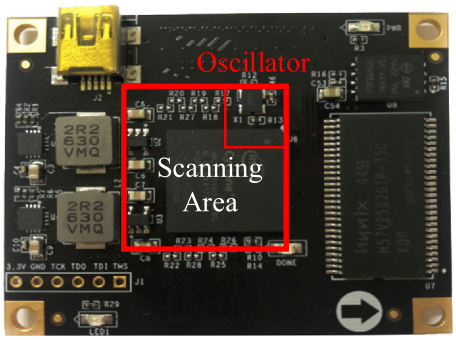

FIGURE 21. The photograph of FPGA.

In addition, a Field Programmable Gate Array (FPGA) as shown in Fig.21 is used to verify this method in engineering application. The size of this board is 50mm × 65mm, and the integrated circuit is driven by an oscillator whose output voltage is 3.3V. The main radiation source is the clock signal at 50MHz and its odd harmonic. The PCB is placed on a large metal alloy plane to reduce the influence of fringe effect. The maximum height of the components is 2.5mm. Therefore, the height of scanning plane is set as 3mm. The scanning area (red line) is 40 mm × 40mm. The spatial resolution of the near-field probe is about 1.9mm at such a height. Therefore, the interval between two neighboring points is set as 2mm at both x and y direction, and the test frequency is 350MHz.

The phase information of near-field data is very difficult to obtain in engineering application. As mentioned in [13], [34], the magnitude-only technique is used to determine an equivalent source. As pointed out in (36), the lack of phase will mitigate the accuracy of the dipole source. But we used more amplitude of near-field data and dipoles to improve the performance of the equivalent solution. Considered the measurement condition of our laboratory in this application, only the amplitude information of near-field data measured by a spectrum analyzer (Agilent) is used to determine an equivalent source.

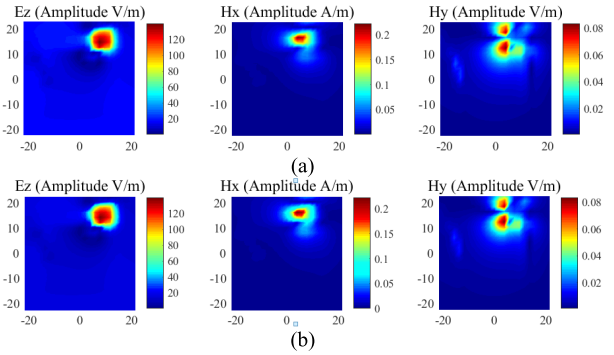

FIGURE 22. (a) Field distribution of the FPGA (b) Calculation results of equivalent dipole source.

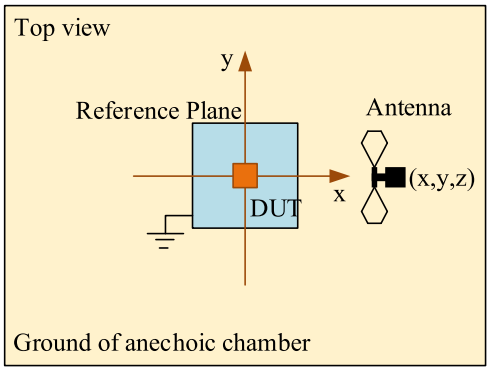

FIGURE 23. The measurement set-up.

TABLE 9. Relative errors of different methods.

Methods	Tikhonov	TSVD	New Method
Error	1.21%	1.97%	0.52%

The target FPGA is working in standby mode, the distribution of the near-field may remain stable or change regularly. The synchronization in the time domain should be considered. Therefore, the time span between two test points should be the integer multiples of the work mode period in time domain. To reduce the measurement error, the perturbation produced by probe is considered firstly. And then, the electric and magnetic probes should be calibrated carefully as mentioned in Section IV-A. Finally, the set-up of spectrum analyzer is optimized to reduce the noise. The compensated data is presented in Fig.22(a).

The amount of the dipoles is set as 23 × 23, the height of dipole plane is set as 2.5mm, and the interval between two closed dipoles is set as 2mm. The equivalent dipole matrix is calculated by the near-field data with the proposed regularization method. The equivalent dipole model is built in Matlab and used to calculate the field on the near-field scanning plane. As shown in Fig.23 (b), the field produced by the dipole model agree well with the scanning data on the same plane. The relative error is given in Table 9.

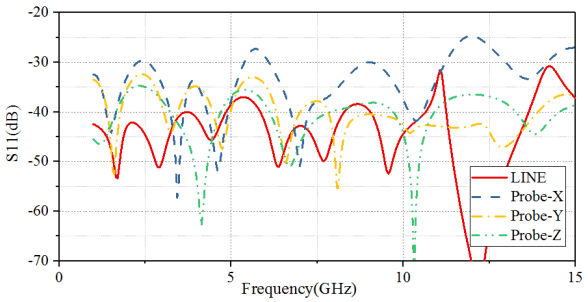

FIGURE 24. The perturbation generated by different electric probes.

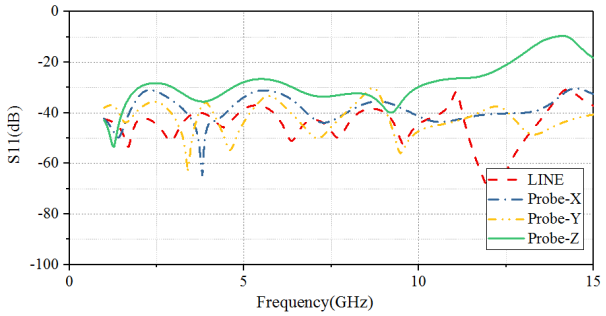

FIGURE 25. The perturbation generated by different magnetic probes.

TABLE 10. Simulation and measurement results.

Antenna Location (x, y, z)(m)	Sim.Ex (dBV/m)	Mea.Ex (dBV/m)	Sim.Ey (dBV/m)	Mea.Ey (dBV/m)
(1, 0, 1)	-63.68	-61.18	-69.00	-63.15
(0, 1, 1)	-62.48	-56.36	-70.56	-65.32
(0, -1, 1)	-62.55	-64.72	-66.69	-72.36
(1, 0, 1.5)	-64.46	-62.25	-71.12	-68.21
(0, 1, 1.5)	-64.67	-59.41	-70.56	-66.25
(0, -1, 1.5)	-64.67	-71.35	-68.03	-65.32

From the result, the location of oscillator can be clearly presented. It is obvious that the distribution of voltage and current can be reflected by the equivalent dipole source. It can be used in noise location and emission estimation.

To illustrate the validation of the equivalent dipole source. The tangential components of electric field at some observation points are measured in anechoic chamber. As shown in Fig.23. The FPGA is placed on a reference ground plane, and the antenna is fixed on a holder which can be moved and adjusted. The height of the DUT is set as 1m. And the height of the antenna is set as 1m and 1.5m, respectively. The field data is measured by the antenna at different observation points.

The equivalent dipole model is built and simulated in Matlab. The comparison results between the simulation and measurement are given in Table 10. And the relative error is given in Table 11. The maximum relative error is less than 9.7%. The reason is composed of two main errors. The first error is introduced by the difference between the dipole model and real DUT. And the error cannot be calculated accurately. The second error is introduced by the difference between measurement data and real data. According to [41], the expanded uncertainty of the measurement system can be used to evaluate the second error. Based on the calculation mentioned in [41], the expanded uncertainty of the measurement is 6.55dB.

TABLE 11. Relative errors of different methods.

Results	Tikhonov	TSVD	New Method
Ex	8.4%	10.8%	6.6%
Ey	9.5%	10.1%	6.6%

V. CONCLUSION

To reconstruct an equivalent dipole source that can represent the radiation emission of compact and complex DUT, the solution will be more accurate with more constrain conditions. However, considering the inevitable difficulties in obtaining the electric field tangential components Ex and Ey, a new transfer model based on the normal component of the electric field is used in this paper. The near-field data measurement time of the proposed model can be reduced by 25% compared with the model mentioned in [16]. In addition, the tangential component can be obtained with the 3D full wave simulation model, the maximum relative error is less than about 10%. A new proposed regularization algorithm which can improve the dipole solution in both accuracy and efficiency is proposed in this paper. For the same model, the relative error of dipole source can decrease about 45.6% and 72% compared with Tikhonov and TSVD. The new proposed transfer model and regularization method were verified by a simulation and measurement.

APPENDIX

To illustrate the perturbations created by different types of near-field probes, a full wave model is built and simulated in HFSS. The S11 (Fig.24 and Fig.25) of a matched microstrip line is given as a reference. And then, different near-field probes are placed above the center of microstrip line. The change of S11 is recorded to illustrate the level of perturbation. It is obvious that the perturbation generated by tangential component electric probe is larger than the normal component electric probe. And the perturbations created by the tangential component magnetic probes are smaller compared with the normal component magnetic probe.

REFERENCES

[1] Z. Yan, W. Liu, J. Wang, D. Su, X. Yan, and J. Fan, "Noncontact wideband current probes with high sensitivity and spatial resolution for noise location on PCB," *IEEE Trans. Instrum. Meas.*, vol. 67, no. 12, pp. 2881–2891, Dec. 2018.

[2] J. Koh, A. De, T. K. Sarkar, H. Moon, W. Zhao, and M. Salazar-Palma, "Free space radiation pattern reconstruction from non-anechoic measurements using an impulse response of the environment," *IEEE Trans. Antennas Propag.*, vol. 60, no. 2, pp. 821–831, Feb. 2012.

[3] J. Yang, J. Koh, and T. K. Sarkar, "Reconstructing a nonminimum phase response from the far-field power pattern of an electromagnetic system," *IEEE Trans. Antennas Propag.*, vol. 53, no. 2, pp. 833–841, Feb. 2005.

[4] P. Li and L. J. Jiang, "Source reconstruction method-based radiated emission characterization for PCBs," *IEEE Trans. Electromagn. Compat.*, vol. 55, no. 5, pp. 933–940, Oct. 2013.

[5] A. Kiaee, R. R. Alavi, R. Mirzavand, and P. Mousavi, "Numerical and experimental assessment of source reconstruction for very near-field measurements with an array of *H* -Field probes," *IEEE Trans. Antennas Propag.*, vol. 66, no. 3, pp. 1311–1320, Mar. 2018.

[6] T. K. Sarkar, "A super-resolution source reconstruction method using free space Green's function," in *Proc. IEEE Int. Conf. Wireless Inf. Technol. Syst.*, Aug. 2010, pp. 1–4.

[7] P. Petre and T. K. Sarkar, "Planar near-field to far-field transformation using an equivalent magnetic current approach," *IEEE Trans. Antennas Propag.*, vol. 40, no. 11, pp. 1348–1356, Nov. 1992.

[8] A. Taaghol and T. K. Sarkar, "Near-field to near/far-field transformation for arbitrary near-field geometry, utilizing an equivalent magnetic current," *IEEE Trans. Antennas Propag.*, vol. 38, no. 3, pp. 536–542, Aug. 1996.

[9] T. K. Sarkar and A. Taaghol, "Near-field to near/far-field transformation for arbitrary near-field geometry utilizing an equivalent electric current and MoM," *IEEE Trans. Antennas Propag.*, vol. 47, no. 3, pp. 566–573, Mar. 1999.

[10] P. Petre and T. K. Sarkar, "Planar near-field to far-field transformation using an array of dipole probes," *IEEE Trans. Antennas Propag.*, vol. 42, no. 4, pp. 534–537, Apr. 1994.

[11] F. Las-Heras, M. R. Pino, S. Loredo, Y. Alvarez, and T. K. Sarkar, "Evaluating near-field radiation patterns of commercial antennas," *IEEE Trans. Antennas Propag.*, vol. 54, no. 8, pp. 2198–2207, Aug. 2006.

[12] J. Pan, H. Wang, X. Gao, C. Hwang, E. Song, H.-B. Park, and J. Fan, "Radio-frequency interference estimation using equivalent dipole-moment models and decomposition method based on reciprocity," *IEEE Trans. Electromagn. Compat.*, vol. 58, no. 1, pp. 75–84, Feb. 2016.

[13] Y.-F. Shu, X.-C. Wei, R. Yang, and E.-X. Liu, "An iterative approach for EMI source reconstruction based on phaseless and single-plane near-field scanning," *IEEE Trans. Electromagn. Compat.*, vol. 60, no. 4, pp. 937–944, Aug. 2018.

[14] J. Zhang, D. Pommerenke, and J. Fan, "Determining equivalent dipoles using a hybrid source-reconstruction method for characterizing emissions from integrated circuits," *IEEE Trans. Electromagn. Compat.*, vol. 59, no. 2, pp. 567–575, Apr. 2017.

[15] G.-Y. Cho, J. Jin, H.-B. Park, H. H. Park, and C. Hwang, "Assessment of integrated circuits emissions with an equivalent dipole-moment method," *IEEE Trans. Electromagn. Compat.*, vol. 59, no. 2, pp. 633–638, Apr. 2017.

[16] Z. Yu, J. A. Mix, S. Sajuyigbe, K. P. Slattery, and J. Fan, "An improved dipole-moment model based on near-field scanning for characterizing near-field coupling and far-field radiation from an IC," *IEEE Trans. Electromagn. Compat.*, vol. 55, no. 1, pp. 97–108, Feb. 2013.

[17] E. Song and H. Ho Park, "A component-level radio-frequency interference evaluation method for mobile devices," *IEEE Trans. Electromagn. Compat.*, vol. 55, no. 6, pp. 1358–1361, Dec. 2013.

[18] K. Kwak, J. Kim, T.-I. Bae, K. Hong, and H. Kim, "Comparison and application of two approaches extracting equivalent dipole arrays of an IC from measured near-field magnitude data," in *Proc. IEEE Electr. Design Adv. Packag. Syst. Symp. (EDAPS)*, Dec. 2018, pp. 1–3.

[19] W. Liu, Z. Yan, and W. Zhao, "Extraction of equivalent dipole-moment model based on improve mapped matrix," in *Proc. 11th Int. Symp. Antennas, Propag. EM Theory (ISAPE)*, Oct. 2016, pp. 504–507.

[20] J. Dong, G. Zhang, Y. Geng, and J. Wang, "Influence of magnetic measurement modeling on the solution of magnetostatic inverse problems applied to current distribution reconstruction in switching air arcs," *IEEE Trans. Magn.*, vol. 54, no. 3, pp. 1–4, Mar. 2018.

[21] T. Sarkar, K. Siarkiewicz, and R. Stratton, "Survey of numerical methods for solution of large systems of linear equations for electromagnetic field problems," *IEEE Trans. Antennas Propag.*, vol. AP-29, no. 6, pp. 847–856, Nov. 1981.

[22] J. Zhang and J. Fan, "Source reconstruction for IC radiated emissions based on magnitude-only near-field scanning," *IEEE Trans. Electromagn. Compat.*, vol. 59, no. 2, pp. 557–566, Apr. 2017.

[23] L. Ghezzi, D. Piva, and L. Di Rienzo, "Current density reconstruction in vacuum arcs by inverting magnetic field data," *IEEE Trans. Magn.*, vol. 48, no. 8, pp. 2324–2333, Aug. 2012.

[24] I. R. Ciric and Y. Qin, "Self-adaptive selection of the regularization parameter for electromagnetic imaging," *IEEE Trans. Magn.*, vol. 33, no. 2, pp. 1556–1559, Mar. 1997.

[25] J. L. A. Quijano and G. Vecchi, "Field and source equivalence in source reconstruction on 3D surfaces," *Prog. Electromagn. Res.*, vol. 103, pp. 67–100, 2010. [Online]. Available: http://www.jpier.org/PIER/pier.php?paper=10030309

[26] M. A. Ali and M. Moghaddam, "3D nonlinear super-resolution microwave inversion technique using time-domain data," *IEEE Trans. Antennas Propag.*, vol. 58, no. 7, pp. 2327–2336, Jul. 2010.

[27] Y. A. Lopez, F. Las-Heras Andres, M. R. Pino, and T. K. Sarkar, "An improved super-resolution source reconstruction method," *IEEE Trans. Instrum. Meas.*, vol. 58, no. 11, pp. 3855–3866, Nov. 2009.

[28] M. S. Zhdanov, *Geophysical Inverse Theory and Regularization Problems*, vol. 36. New York, NY, USA: Elsevier, 2002.

[29] J. D. Shea, B. D. Van Veen, and S. C. Hagness, "A TSVD analysis of microwave inverse scattering for breast imaging," *IEEE Trans. Biomed. Eng.*, vol. 59, no. 4, pp. 936–945, Apr. 2012.

[30] F. Luan, C. Lee, J.-H. Choi, and H.-K. Jung, "A comparison of regularization techniques for magnetoencephalography source reconstruction," *IEEE Trans. Magn.*, vol. 46, no. 8, pp. 3209–3212, Aug. 2010.

[31] J.-R. Regue, M. Ribo, J. Gomila, A. Perez, and A. Martin, "Modeling of radiating equipment by distributed dipoles using metaheuristic methods," in *Proc. Int. Symp. Electromagn. Compat.*, Aug. 2005, pp. 596–601.

[32] W.-J. Zhao, B.-F. Wang, E.-X. Liu, H. B. Park, H. H. Park, E. Song, and E.-P. Li, "An effective and efficient approach for radiated emission prediction based on amplitude-only near-field measurements," *IEEE Trans. Electromagn. Compat.*, vol. 54, no. 5, pp. 1186–1189, Oct. 2012.

[33] H. Fan, "Far field radiated emission prediction from magnetic near field magnitude-only measurements of PCBs by genetic algorithm," in *Proc. IEEE Int. Symp. Electromagn. Compat.*, Aug. 2009, pp. 321–324.

[34] F. Las-Heras and T. K. Sarkar, "A direct optimization approach for source reconstruction and NF-FF transformation using amplitude-only data," *IEEE Trans. Antennas Propag.*, vol. 50, no. 4, pp. 500–510, Apr. 2002.

[35] D. Watzenig, B. Brandstatter, and G. Holler, "Adaptive regularization parameter adjustment for reconstruction problems," *IEEE Trans. Magn.*, vol. 40, no. 2, pp. 1116–1119, Mar. 2004.

[36] D. Baudry, C. Arcambal, A. Louis, B. Mazari, and P. Eudeline, "Applications of the near-field techniques in EMC investigations," *IEEE Trans. Electromagn. Compat.*, vol. 49, no. 3, pp. 485–493, Aug. 2007.

[37] X. Tong, D. W. P. Thomas, A. Nothofer, P. Sewell, and C. Christopoulos, "Modeling electromagnetic emissions from printed circuit boards in closed environments using equivalent dipoles," *IEEE Trans. Electromagn. Compat.*, vol. 52, no. 2, pp. 462–470, May 2010.

[38] D. W. P. Thomas, K. Biwojno, T. Xin, A. Nothofer, P. Sewell, and C. Christopoulos, "Measurement and simulation of near field emissions from microstrip lines," in *Proc. Int. Symp. Electromagn. Compat. (EMC Eur.)*, Sep. 2008, pp. 1–6.

[39] C. A. Balanis, *Antenna Theory: Analysis and Design*, vol. 1, 3rd ed. Hoboken, NJ, USA: Wiley, 2005.

[40] *IEEE Standard for Calibration of Electromagnetic Field Sensors and Probes (Excluding Antennas) From 9 kHz to 40 GHz*, IEEE Standard 1309, Nov. 2013.

[41] *Specification for Radio Disturbance and Immunity Measuring Apparatus and Methods—Part 4–2: Uncertainties, Statistics and Limit Modelling—Measurement Instrumentation Uncertainty*, Standard BS EN 55016-4-2:2011, Oct. 2011.

WEI LIU was born in Anyang, China, in 1993. He received the B.S. degree in information warfare technology from Harbin Engineering University, Harbin, China, in 2015. He is currently pursuing the Ph.D. degree in electronic science and technology with Beihang University, Beijing, China.

His current research interests include the development of near field measurement technique, the study of near-field probe, and EMI source reconstruction.

ZHAOWEN YAN received the B.S. degree from Henan Polytechnic University, in 1991, the M.S. degree from the Xi'an University of Science and Technology, in 1996, and the Ph.D. degree in electrical engineering from Xi'an Jiaotong University, China, in 1999.

From 1999 to 2002, he was a Postdoctoral Research Associate with the Huazhong University of Science and Technology. From April 2003 to May 2005, he holds a postdoctoral position at Beihang University and from December 2012 to December 2013, he was a Visiting Scholar with the EMC Laboratory, Missouri University of Science and Technology, USA. He is currently a Professor of electronic science and technology with Beihang University. He has published more than 100 conferences and journal articles and eight monographs on electromagnetic theory. He has 32 authorized patents. For many years, his research activity was focused on the electromagnetic field computation and EMC analysis. He received the First Prize of the Natural Science of the Ministry of Education of PRC, in 2003, and the National Defense Science and Technology Progress, in 2011, as recognition of his research work. He received the Second Prize for the National Science and Technology Progress, in 2012, and also the First Prize for National Defense Technology Invention, in 2017. He won the First Prize of the National Technology Invention, in 2018.

JIANWEI WANG received the B.S. degree in electronic information engineering from the Civil Aviation University of China, in 2014, and the M.S. degree in electronic science and technology from Beihang University, in 2017, where he is currently pursuing the Ph.D. degree in electronic science and technology.

His current research interests include near-field probe and near-field measurement.

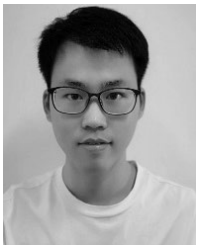

ZHENG MIN received the B.S. degree in electronic information engineering from Harbin Engineering University, Harbin, China, in 2018. He is currently pursuing the M.S. degree in electronic science and technology with Beihang University, Beijing, China.

His current research interests include high-speed acquisition and analysis of EMC elements.

ZHANGQIANG MA received the B.S. degree in electronic information engineering from Beihang University, Beijing, China, in 2018, where he is currently pursuing the Ph.D. degree in electronic science and technology.

His current research interests include signal integrity analysis and near-field measurement.